Water Science and Engineering 2019, 12(3): 235–243

HOSTED BY

ELSEVIER

Available online at www.sciencedirect.com

Water Science and Engineering

journal homepage: http://www.waterjournal.cn

Influence of bed elevation discordance on flow patterns and head losses in an open-channel confluence

Pedro Xavier Ramos [a,*], Laurent Schindfessel [a], João Pedro Pêgo [b], Tom De Mulder [a]

[a] *Department of Civil Engineering, Ghent University, Ghent 9000, Belgium*
[b] *Faculty of Engineering, University of Porto, Porto 4200-465, Portugal*

Received 16 January 2019; accepted 22 May 2019
Available online 10 September 2019

Abstract

Confluences play a major role in the dynamics of networks of natural and man-made open channels, and field measurements on river confluences reveal that discordance in bed elevation is common. Studies of schematized confluences with a step at the interface between the tributary and the main channel bed reveal that bed elevation discordance is an important additional control for the confluence hydrodynamics. This study aimed to improve understanding of the influence of bed elevation discordance on the flow patterns and head losses in a right-angled confluence of an open channel with rectangular cross-sections. A large eddy simulation (LES)-based numerical model was set up and validated with experiments by others. Four configurations with different bed discordance ratios were investigated. The results confirm that, with increasing bed elevation discordance, the tributary streamlines at the confluence interface deviate less from the geometrical confluence angle, the extent of the recirculation zone (RZ) gets smaller, the ratio of the water depth upstream to that downstream of the confluence decreases, and the water level depression reduces. The bed elevation discordance also leads to the development of a large-scale structure in the lee of the step. Despite the appearance of the large-scale structure, the reduced extent of the RZ and associated changes in flow deflection/contraction reduce total head losses experienced by the main channel with an increase of the bed discordance ratio. It turns out that bed elevation discordance converts the lateral momentum from the tributary to streamwise momentum in the main channel more efficiently.

Keywords: Open channel confluence; Bed elevation discordance; Three-dimensional numerical modelling; Large eddy simulation; Recirculation zone

1. Introduction

Stream confluences play an important role in networks of natural or artificial open channels, as they regulate water elevations and transport of sediments, nutrients, and pollutants. Therefore, confluence hydrodynamics has been the subject of many field studies, laboratory experiments, and numerical simulations (Rice et al., 2008; Konsoer and Rhoads, 2014; Gualtieri et al., 2018; Yuan et al., 2017, 2018; Umar et al., 2018; Lewis and Rhoads, 2018). Bathymetric surveys in river confluences often reveal the existence of a difference in bed elevation between the tributary and the main open channel (Kennedy, 1983, 1984; Biron et al., 1996a). Moreover, the flow patterns of discordant bed confluences are found to be profoundly different from those of concordant bed confluences (Biron et al., 1996a, 1996b; Bradbrook et al., 2001). Field studies by De Serres et al. (1999) and Boyer et al. (2006) indicate that a strong secondary circulation may develop in the lee of a bed elevation discordance in the confluence hydrodynamic zone (CHZ). This feature may not only be

* Corresponding author.
E-mail address: Pedro.Ramos@ugent.be (Pedro Xavier Ramos).
Peer review under responsibility of Hohai University.

https://doi.org/10.1016/j.wse.2019.09.005

relevant to mixing and scouring processes, but its interaction with the other features of the open-channel confluence may be important for the head losses, hence the backwater effects induced by the confluence. Also, laboratory experiments have revealed significant differences in flow and turbulence characteristics between discordant and concordant bed confluences (Biron et al., 1996a; 1996b).

Detailed laboratory (e.g., Weber et al., 2001; Creëlle et al., 2017; Yuan et al., 2018) and numerical studies (e.g., Constantinescu et al., 2012, 2014; Luo, 2017) of the hydrodynamics of asymmetric confluences of open channels with equal width often make use of geometrically schematized configurations with sharp-edged confluence corners. In the case of concordant beds, such confluences are characterized by complex hydrodynamic patterns (Fig. 1(a), which is modified based on Best (1987)), including a zone of flow stagnation at the upstream confluence corner, a mixing layer between the merging flows, a separation zone of flow from the downstream confluence corner (Hager, 1987), and an ensuing shear layer (Best, 1987). Those patterns are predominantly influenced by parameters, such as the geometrical confluence angle, the momentum flux ratio, the cross-sectional shape, and the Froude number (Fr) of the downstream channel. As mentioned above, the flow patterns are also significantly influenced by the bed elevation discordance, which is often modelled as a sharp step at the interface between the tributary and the main channel (e.g., Biron et al., 1996a; Đorđević, 2013) (Fig. 1(b)).

Notwithstanding the relatively high-resolution data acquired in laboratory experiments of confluences with concordant (e.g., Weber et al., 2001) or discordant beds (e.g., Biron et al., 1996b), these experimental datasets do not allow for quantitative characterization of all important flow structures. Actually, there is still some controversy regarding the flow structure of open channel confluences, as discussed by Rice et al. (2008), Pouchoulin et al. (2018), and Ramos et al. (2019). Biron et al. (1996b) have also shown that some intermittent phenomena are not easily captured in experiments. As Biron et al. (1996b) and Bradbrook et al. (2001) explained, the flow structure in open-channel confluences contains unstable phenomena, and the monitoring of such features requires a dense array of simultaneous velocity measurements. Therefore, numerical tools are important in producing additional data for the study of the CHZ. Discordant bed confluences have been studied based on a Reynolds-averaged Navier-Stokes (RANS) model (e.g., Huang et al., 2002; Đorđević, 2013) or tools based on eddy-resolving methods, such as large eddy simulation (LES) (e.g., Bradbrook et al., 2010). The use of LES for the study of open-channel confluences was motivated by Bradbrook et al. (2010), Schindfessel et al. (2015), and Ramos et al. (2019). In LES, the flow and turbulence are for the most part resolved on the mesh (Rodi, 2017), which enables a more thorough study of hydrodynamics in an open-channel confluence.

The aim of the present study was to investigate with LES simulations the effect of differences in bed elevations between the tributary and main channel on confluence hydrodynamics in a right-angled open-channel confluence. Specifically, the impacts on flow deflections, recirculation zone dimensions, and secondary flow in the lee of the step were examined. Ultimately, the effect of those flow patterns on the open-channel confluence head losses was investigated.

First a concordant bed case studied experimentally by Weber et al. (2001) was simulated to validate the numerical model. Then, the tributary in the model was made shallower by introducing a sharp discordant step. Three simulations with different bed discordance ratios were carried out. Each discordant ratio corresponded to a different phase within the scouring process in nature, and normally, the final bed elevation discordance did not exceed 50% of the water depth downstream of the confluence zone (Kennedy, 1983).

2. Numerical methodology and model verification

2.1. Numerical framework

The numerical simulations in the present study were conducted with OpenFOAM version 5.0, which is an open-source computational fluid dynamics (CFD) software programmed in C++. This toolbox provides a flexible and programmable environment, and can be used to solve the governing equations

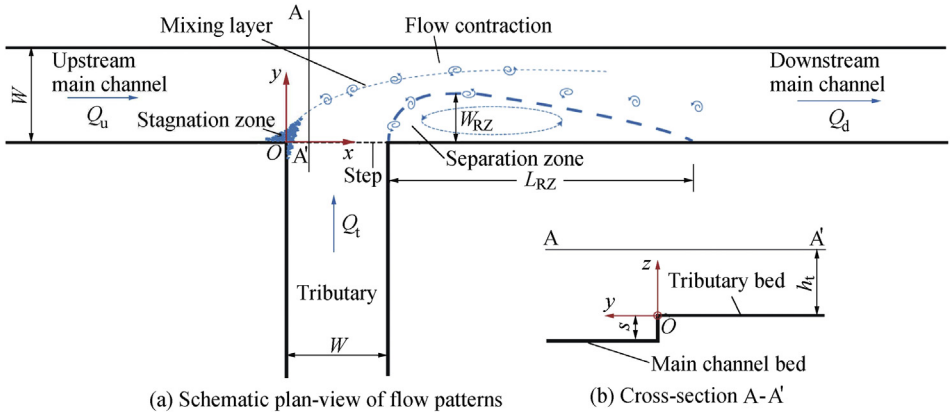

Fig. 1. Flow patterns in a right-angled open-channel confluence.

for an incompressible, viscous flow. To model the turbulent nature of these flows, LES was used in this study. As a subgrid-scale (SGS) model, the standard Smagorinsky model was used, with a constant C_s of 0.158 (Rodi et al., 2013; Schindfessel et al., 2015). Further details of this model can be found in Schindfessel et al. (2015) and Ramos et al. (2019).

2.2. Hydraulic conditions

First, a confluence with a concordant bed in an open channel, with a width of $W = 0.914$ m, was simulated, for which experimental data were available. More specifically, the case of Weber et al. (2001), with a discharge ratio of $q = 0.58$, was used to validate the numerical model, where $q = Q_u/Q_d = Q_u/(Q_u + Q_t)$, with Q_u, Q_d, and Q_t being the discharges of the upstream and downstream main channel and tributary of the open channel, respectively. Then, the model geometry was modified by introducing a step at the interface between the tributary and the main channel to elevate the bed level of the tributary. The bed discordance ratio or relative step height (σ) is defined as $\sigma = s/h_d$, where s is the step height, and h_d is the downstream water depth. Three configurations with different bed discordance ratios ($\sigma = 0.10$, $\sigma = 0.25$, and $\sigma = 0.50$) were simulated. For each of the discordant bed cases, the downstream water depth (h_d) and the discharges in the branches of the confluence (Q_u and Q_t) were kept identical to the values adopted in the concordant bed case ($\sigma = 0$) in this study, i.e., $h_d = 0.308$ m, and $Q_d = 0.170$ m^3/s. As a consequence, the discharge ratio was identical for all cases, but the flow velocity in the tributary (U_t) increased with σ (Table 1). This is a common approach in the study of open-channel confluences with discordant beds (Biron et al., 1996a, 1996b; Đorđević, 2013). The study cases, sharing the same Froude and Reynolds (Re) numbers, with $Fr = 0.37$, and $Re = 111000$, are shown in Table 1.

Table 1
Study cases.

σ	U_t/U_d	σ	U_t/U_d
0	0.418	0.25	0.557
0.10	0.464	0.50	0.836

Note: U_d is the flow velocity in the downstream main channel.

2.3. Computational meshes

The computational domain was discretized by means of structured meshes. The numbers of the cells in the main channel and in the tributary are presented in Table 2. The meshes were graded such that a higher resolution was obtained in the confluence zone.

2.4. Boundary conditions

In order to obtain a fully developed turbulent inflow in the main and tributary channels, the inlet velocities were simulated by means of a periodic boundary condition (Fig. 2). A fraction of random turbulence was added. As the downstream outlet boundary condition, the pressure was specified and a Neumann boundary condition was imposed on velocity. The boundary layers along the glass walls were not fully resolved, but the LES computations were combined here with a three-layer model (Schindfessel et al., 2015).

Regarding the treatment of the free surface, given the moderately low Froude number ($Fr < 0.37$), the numerical treatment was done by means of a flat rigid lid. The advantages and shortcomings of such an approach were debated for the same geometry with a tributary-dominant discharge ratio in Ramos et al. (2019). In contrast to that case ($q = 0.25$), the three-dimensional (3D) flow in the hydraulic conditions in this study ($q = 0.58$) did not suffer from limitations of over-simplification in a substantial way. Therefore, the presented results are based on simulations, in which the free surface was treated as a flat, horizontal, and frictionless rigid lid at the top boundary, which was located at a vertical distance h_d and h_t ($h_t = h_d - s$) above the bed of the main channel and the tributary, respectively. For discussion on the rigid-lid approach in other flow cases, see Constantinescu et al. (2012) and Kara et al. (2015).

2.5. Model verification

For the verification of the numerical model, the guidelines of Pope (2004), Lane et al. (2005), and Blocken and Gualtieri (2012) were largely relied upon.

2.5.1. Intended use and specification of modelling

Given the ultimate goal of the present study, i.e., investigating the influence of bed elevation discordance on head

Table 2
Numbers of mesh cells.

σ	Result of main channel						Result of tributary						Total number of cells
	Longitudinal		Lateral		Vertical		Longitudinal		Lateral		Vertical		
	Length (m)	Number of cells	Width (m)	Number of cells	Height (m)	Number of cells	Length (m)	Number of cells	Width (m)	Number of cells	Height (m)	Number of cells	
0	11.882	1130	0.914	90	0.308	45	4.57	500	0.914	90	0.308	45	6601500
0.10	11.882	1130	0.914	90	0.308	45	4.57	500	0.914	90	0.277	40	6376500
0.25	11.882	1130	0.914	90	0.308	45	4.57	500	0.914	90	0.231	34	6106500
0.50	11.882	1130	0.914	90	0.308	45	4.57	500	0.914	90	0.154	23	5611500

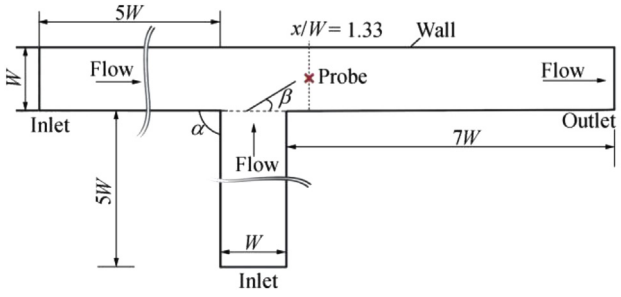

Fig. 2. Boundary conditions and dimensions of numerical domain (probe is at half-depth, with $z = h_d/2$).

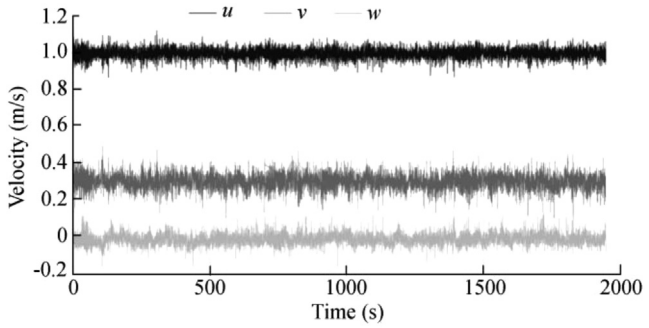

Fig. 3. Velocity components at location of $x = 1.33\ W$, $y = W/2$, and $z = h_d/2$.

losses in the CHZ, the purpose of the numerical model was, therefore, to simulate as accurately as possible the recirculation zone (RZ) dimensions and the other secondary flow patterns in time-averaged flow fields.

2.5.2. Estimation of performance criteria and conditional verification

2.5.2.1. Mesh independency test

The meshes used in this study (section 2.3) were defined on the basis of a mesh sensitivity and independency analysis, as well as on the validation described in section 3.1.

2.5.2.2. Determination of solution convergence, solution accuracy in time, initialization, and averaging time

The governing equations were discretized by means of the finite volume method, adopting second-order accurate schemes in time and space. The resulting equations were solved in a segregated process using an iterative sequence and coupled using the pressure-implicit with splitting of operators (PISO) algorithm. In all the four simulations, the time step equalled 0.025 s, resulting in an average Courant-Friedrichs-Lewy (CFL) number of about 0.15 and a maximum CFL number of about 1.5. Note that the adopted implicit time stepping method was unconditionally stable. For further details about the choice of numerical parameters in the present model, see Schindfessel et al. (2015).

To obtain the LES results in this study, the simulations advanced more than 600 s before the data collection started. This initialization time corresponded to $33T$ (where $T = 12W/U_d$ is an approximate flow-through time for the main channel with a length of $12W$). Data collection and time averaging spanned an additional $75T$ of simulation (1350 s). Fig. 3 shows the instantaneous velocity components along those intervals of time in the middle of a cross-section of the main channel located slightly downstream of the confluence (at the probe indicated in Fig. 2). In Fig. 3, u, v, and w are the flow velocity components in the streamwise, lateral, and vertical directions, respectively. A fast Fourier transform (FFT) analysis was carried out, without any dominant frequency being found.

2.5.2.3. Wall-normal distance of first grid cell

As a consequence of the use of wall functions, the dimensionless wall-normal distance of the first grid cells (y^+) along the sidewalls and the bed should meet the criterion of $30 < y^+ < 300$ (Keylock et al., 2012). This condition was met for all the simulations, with y^+ being usually above 30, except for the zones of low flow velocity. These minor exceptions were expected and accepted, especially in the stagnation zone (McSherry et al., 2017; Schindfessel et al., 2015; Schindfessel, 2017).

2.5.2.4. Verification of turbulent kinetic energy (TKE) being sufficiently resolved

Since LES is based on the assumption that the subgrid scales can be modelled by an SGS model, Pope (2004) recommended that at least 80% of the TKE (k_{res}) is resolved on the mesh, according to Eq. (1). Fig. 4 shows that more than 80% of the cells, in each of the four simulations, meet Pope's criterion.

$$k_{res} = \frac{1}{2}\left(\overline{u'^2} + \overline{v'^2} + \overline{w'^2}\right) \tag{1}$$

where u', v', and w' are the velocity fluctuations in the streamwise, lateral, and vertical directions, respectively; and the overbars represent time-averaging.

2.5.3. Computational resources and time

The simulations were computed on a 4 × 8-core Intel Xeon E5-2670 (Sandy Bridge @2.6 GHz) at Ghent University. The total computational expense of a simulation was roughly 4600 CPU hours. An advantage of OpenFOAM is the parallelized code at a fundamental level, allowing for easy programming and running in parallel. In this study, the numerical domain was decomposed into 32 sub-domains. Therefore, the real computational time was about 144 h for each simulation.

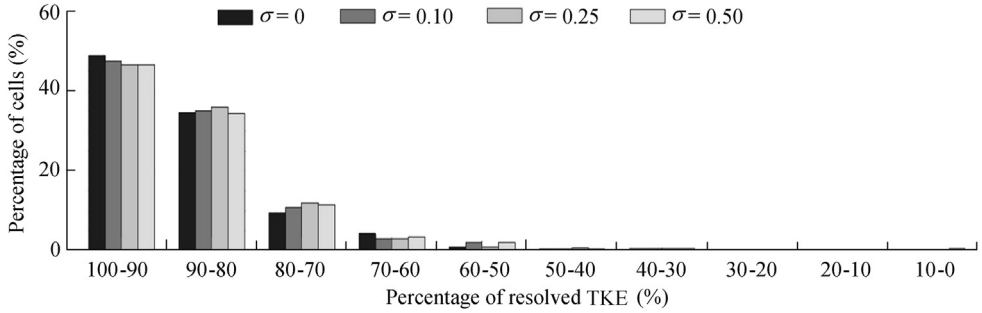

Fig. 4. Percentage of TKE resolved on mesh for each of four simulations.

3. Results and discussion

3.1. Validation against experimental data for concordant bed case

First, the numerical model was validated with the experimental data of water depth (h) for the concordant bed case ($\sigma = 0$) acquired by Weber et al. (2001). Fig. 5 shows the agreement between the measured water depths and the numerically predicted water depths in the symmetry plane ($y/W = 0.5$) of the main channel, where the latter were obtained by converting the predicted time-averaged pressures on the rigid lid to those on a virtual free surface (Rodi et al., 2013; Ramos et al., 2019).

A comparison of measured and predicted profiles of the time-averaged streamwise velocity component (U) at five different locations along the symmetry plane in the main channel is shown in Fig. 6. The overall agreement is fair, although the water level depression in the flow contraction zone was slightly underestimated (Fig. 5(c)). However, the velocity dip near $z/h_d \approx 1$ was only captured by the model at the locations of $x/W \geq 2.33$, and the model did not capture the velocity dip in the near-bed region around $z/h_d \approx 0.1$.

The TKE profiles at five locations along the plane of $y/W = 0.125$ of the main channel, which contains the higher turbulent kinetic energy, are presented in Fig. 7, in which k_{res} is nondimensionalized with respect to U_d^2, i.e., $k^* = k_{res}/U_d^2$. Some differences are noticeable, which may be partially due to the lower temporal resolution of the acoustic Doppler velocimetry measurements in Weber et al. (2001), as mentioned in Huang et al. (2002).

3.2. Concordant vs. discordant beds

With the validated model, the three cases of bed elevation discordance ($\sigma = 0.10$, $\sigma = 0.25$, and $\sigma = 0.50$) were simulated.

The predicted water depths along three longitudinal transects of the main channel for the concordant and two discordant bed cases are shown in Fig. 8. It can be seen that, with an increase of the bed discordance ratio, the water level depression in the flow contraction zone becomes smaller. Note that the ratio of the water depth upstream to that downstream of the confluence also decreases when the height of the step increases.

Fig. 9 gives an overall impression of the streamlines originating from the tributary flow for the cases $\sigma = 0$ and $\sigma = 0.25$. These streamlines were initiated at an elevation of 50% of the water depth h_d above the main channel bed.

In both $\sigma = 0$ and $\sigma = 0.25$ cases, the streamlines start to deviate from the longitudinal axis of the tributary before the tributary flow reaches the confluence interface. This causes the flow angle β (as shown in Fig. 2) at the confluence interface to deviate from the geometrical confluence angle ($\alpha = 90°$).

For different bed discordance ratios ($\sigma = 0$, $\sigma = 0.10$, $\sigma = 0.25$, and $\sigma = 0.50$), the variations of β at different elevations above the corresponding tributary bed are shown in Fig. 10. It can be seen that the flow angle β increases with the bed discordance ratio at different elevations, which means that the tributary flow is less deflected with an increasing bed discordance ratio, as was found in the RANS-based model results of Đorđević (2013). These findings are related to the 3D complex flow effects due to the interaction of the merging flows and the

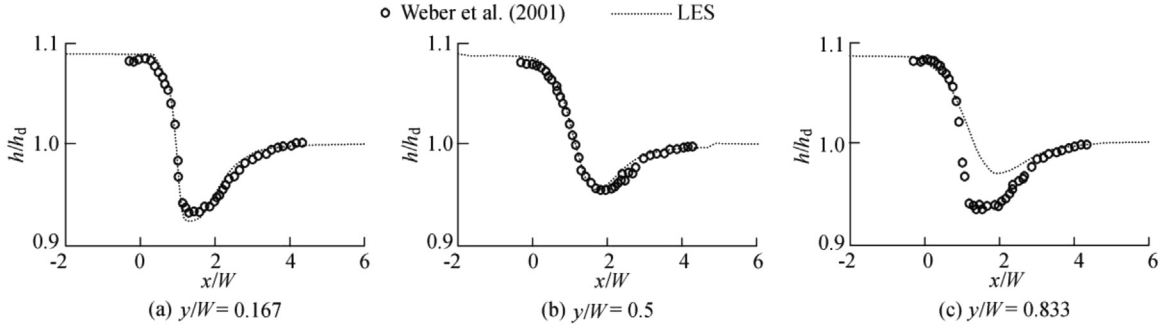

Fig. 5. Comparison of predicted and measured water depths for different longitudinal transects of main channel in concordant bed case.

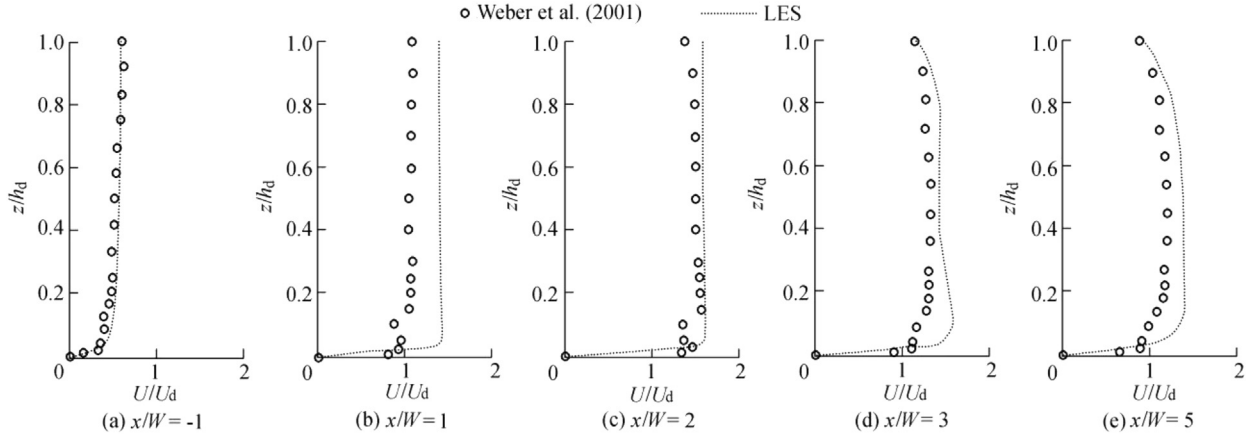

Fig. 6. Comparison of predicted and measured time-averaged streamwise velocity profiles at different locations (x/W) along symmetry plane ($y/W = 0.5$) of main channel in concordant bed case.

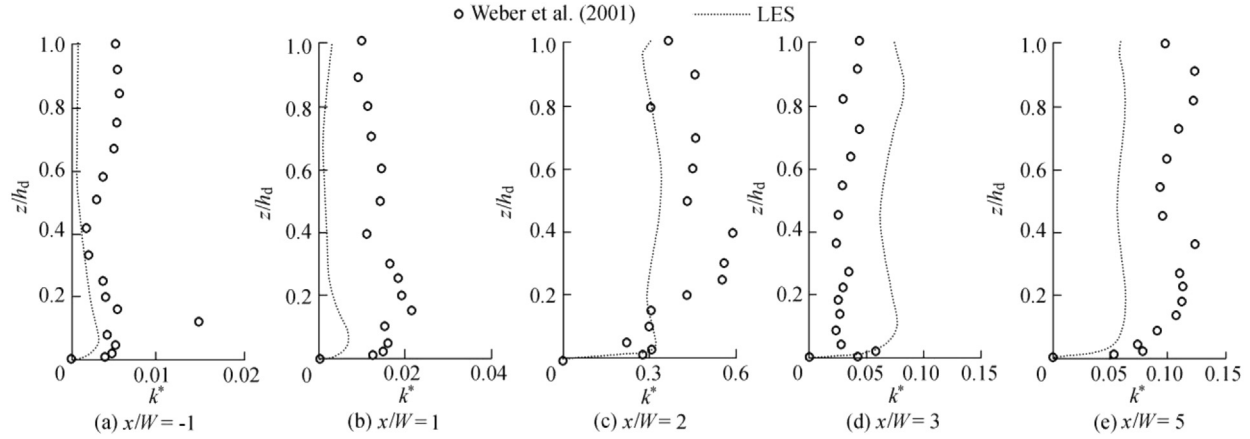

Fig. 7. Comparison of measured and predicted TKE profiles at different locations (x/W) along plane of $y/W = 0.125$ of main channel in concordant bed case.

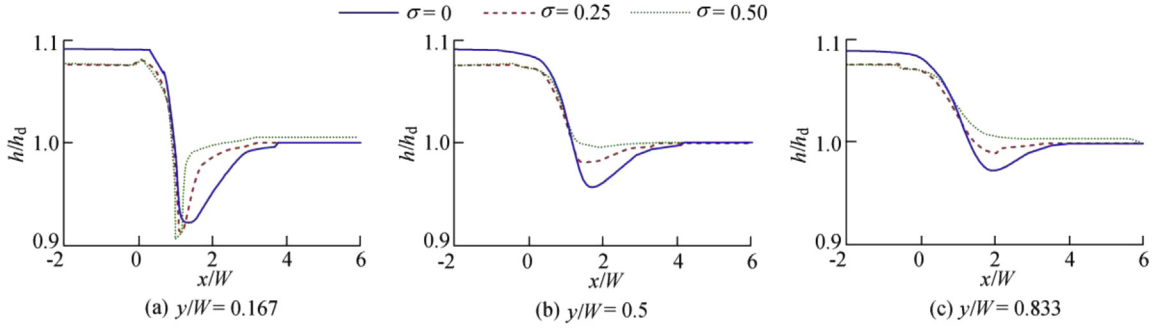

Fig. 8. Water depths along three longitudinal transects calculated with pressures on rigid lid for simulations in different cases.

step (including upwelling effects, visible in Fig. 9), as well as to the increase of the tributary flow velocities with increasing step height (section 2.2).

Fig. 9 also reveals that in both the concordant and discordant bed cases, the tributary flow separates at the downstream confluence corner, forming an RZ. The dimensions of the RZ can be delineated from the predicted velocity fields in different manners (Schindfessel et al., 2015). Here, the so-called isovel method is applied, which delineates the dimensions of the RZ by means of the line of zero longitudinal velocity. The lengths (L_{RZ}) and the maximum widths (W_{RZ}) of the RZ are shown in Fig. 11.

Note that in Fig. 11 the RZ dimensions become smaller for a higher discordance ratio. This is also visible in Fig. 12,

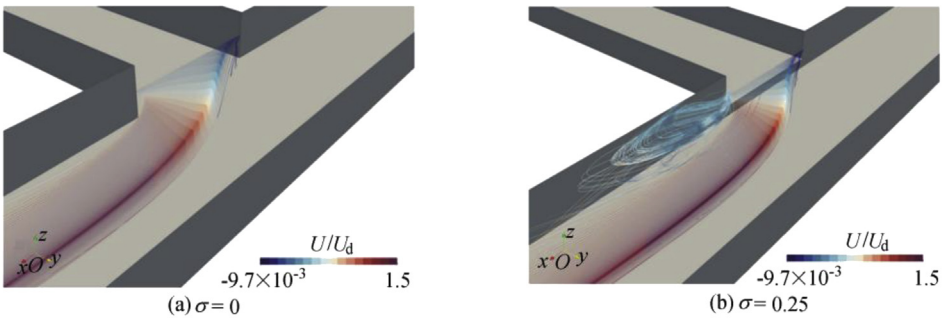

Fig. 9. Streamlines originating from tributary flow for different bed discordance cases.

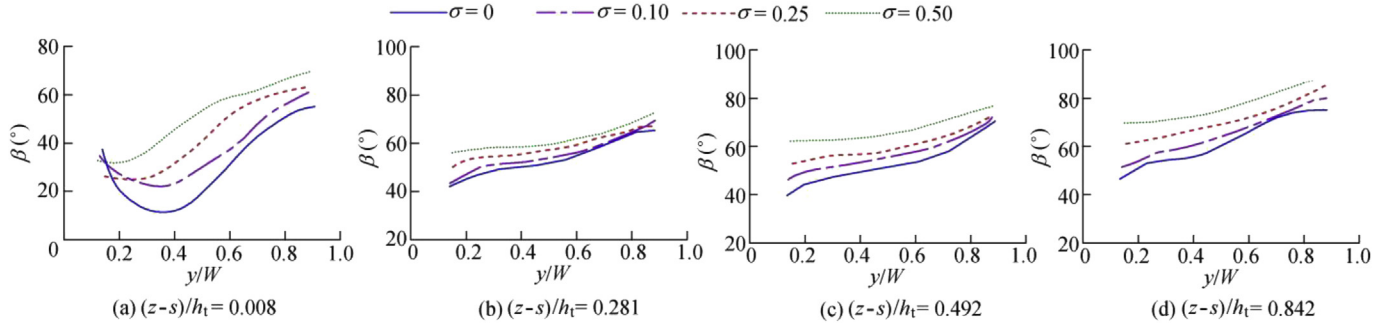

Fig. 10. Flow angles at different elevations of interface between tributary and main channel, defined according to conventional depiction.

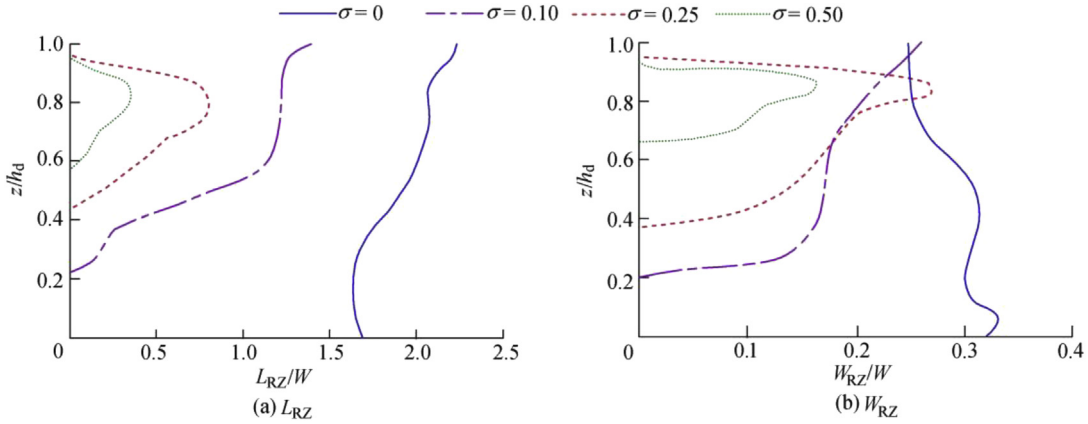

Fig. 11. Dimensions of RZ determined by isovel method for different bed discordance ratios.

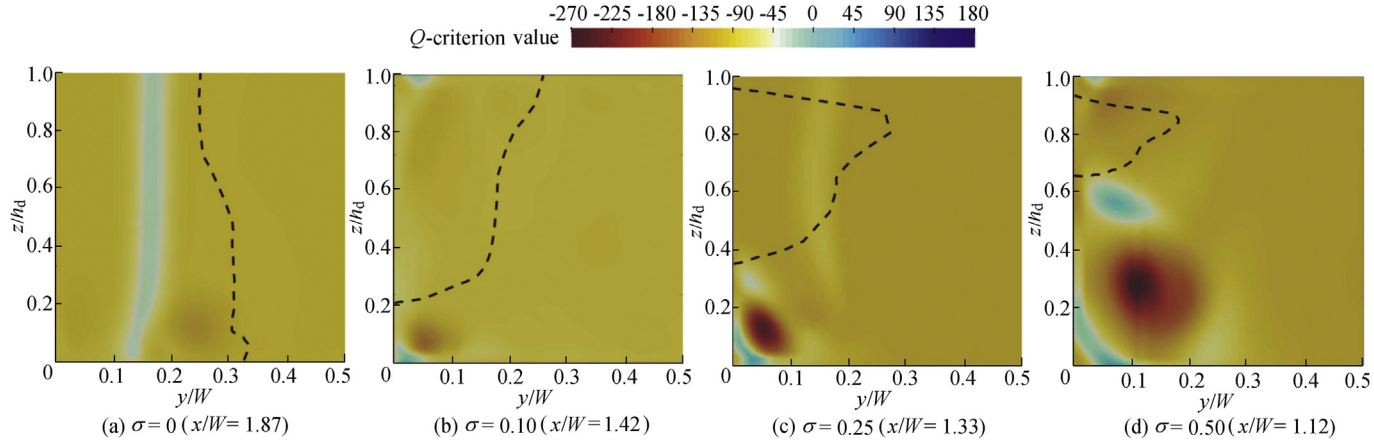

Fig. 12. Q-criterion contours and RZ widths in halved cross-section of maximum RZ width based on time-averaged flow velocity.

Table 3
Head loss coefficient for main channel.

σ	ξ_m	σ	ξ_m
0	0.374	0.25	0.206
0.10	0.352	0.50	0.086

where, for each of the four cases, the extent of the RZ is shown (dashed line) in the cross-section pertaining to its maximum width. It is apparent from Fig. 12 that the location of the maximum RZ width moves closer to the confluence when the bed elevation discordance increases. Unlike $\sigma = 0$ and $\sigma = 0.10$ cases, where the RZ exists up to the upper boundary (i.e., the flat rigid lid), the RZ in $\sigma = 0.25$ and $\sigma = 0.50$ cases does not exist near that boundary. The results in Fig. 11 also suggest that there are no conditions for the development of an RZ at elevations below the tributary bed level, which is related to the upwelling flow near the downstream confluence corner (see Fig. 9). This observation agrees with the RANS-based model results of Đorđević (2013). Besides the detachment at the downstream confluence corner and the subsequent formation of the RZ, the tributary flow in discordant bed cases also detaches from the brink of the step. Due to the interaction with the flow coming from the upstream main channel, a large-scale structure develops in the lee of the step and below the RZ. Instead of quantifying the secondary flow by means of a vertical gradient of transversal velocity components (e.g., Karami et al., 2017), the aforementioned large-scale structure that passes underneath the RZ is visualized (colour plots in Fig. 12) by means of the so-called Q-criterion (Hunt et al., 1988; Dubief and Delcayre, 2000). The Q-criterion makes use of the time-averaged velocity gradient tensor to visualize coherent flow motion. Note that in the cases with bed discordance, the size of the 3D vortex tube has a diameter roughly equal to the corresponding step height. The strength of the associated vorticity, i.e., the magnitude of the Q-criterion value, also seems to grow with the bed discordance ratio.

The complex flow patterns in the CHZ affect head losses. In the concordant bed case, the flow in the main channel experiences head losses that are mainly due to the presence of the RZ (contraction-expansion). Due to the reduced size of the RZ in the discordant bed case, the associated head losses should decrease. However, the appearance of the large-scale structure (Fig. 12) and other changes in the secondary flow patterns may lead, in principle, to additional head losses. Therefore, the influence on the total head losses, induced by the bed elevation discordance, needs to be assessed. To this end, the head differences between the main channel's cross-sections at $x/W = -2$ and $x/W = 6$ were determined, where the head in a cross-section was obtained by integrating the total time-averaged pressures (i.e., the sum of the static and dynamic pressures) over the cross-sectional area. For each of the four simulations, the head difference was nondimensionalized by the cross-sectionally averaged velocity at $x/W = 6$ (which was equal to 0.604 m/s for all the four simulations). The corresponding head loss coefficients (ξ_m, with the formula shown in Ramos et al. (2018)) are presented in Table 3 and can be seen to decrease with the bed discordance ratio.

The observed decrease of head losses with the increasing bed discordance ratio agrees with Fig. 8, where the ratio of the water depth upstream to that downstream of the confluence was also found to decrease with an increase of the bed discordance ratio.

4. Conclusions

(1) The angles of the tributary streamlines at the confluence interface deviate less from the geometrical confluence angle (90°) with the increasing bed elevation discordance. This is due to the complex 3D flow features near the interface between the tributary and the main channel, as well as the increase of tributary flow velocities as the discharge ratio is maintained constant.

(2) An increase in bed elevation discordance leads the tributary flow into the RZ, which is shallower and situated at a higher elevation above the bed of the main channel. With the increase of the bed discordance ratio, the ensuing 3D flow yields, among other effects, a smaller extent of the RZ. The location of the maximum RZ width shifts towards the confluence. For higher bed discordance ratios, i.e., $\sigma \geq 0.25$, the size of the RZ is reduced and even gets eliminated in the proximity of the free surface. In the presence of bed elevation discordance, the RZ vanishes below the level of the tributary bed.

(3) The head losses over the confluence zone of the main channel decrease with the increasing bed discordance ratio. This reduction is caused by two counter effects: an increase in head losses due to the formation of the large-scale structure in the lee of the step, and a larger decrease in head losses due to the formation of a smaller RZ.

Acknowledgements

We are grateful to Ghent University for providing the high-performance computing facilities in the present work.

References

Best, J.L., 1987. Flow dynamics at river channel confluences: Implications for sediment transport and bed morphology. In: Ethridge, F.G., Flores, R.M., Harvey, M.D., eds., Recent Developments in Fluvial Sedimentology. Society for Sedimentary Geology, Tulsa, pp. 27−35. https://doi.org/10.2110/pec.87.39.0027.

Biron, P., Roy, A.G., Best, J.L., 1996a. Turbulent flow structure at a concordant and discordant open channel confluences. Exp. Fluid 21, 437−446. https://doi.org/10.1007/BF00189046.

Biron, P., Best, J.L., Roy, A.G., 1996b. Effects of bed discordance on flow dynamics at open channel confluences. J. Hydraul. Eng. 122(12), 676−682. https://doi.org/10.1061/(ASCE)0733-9429(1996)122:12(676).

Blocken, B., Gualtieri, C., 2012. Ten iterative steps for model development and evaluation applied to computational fluid dynamics for environmental fluid mechanics. Environ. Model. Softw. 33(7), 1−22. https://doi.org/10.1016/j.envsoft.2012.02.001.

Boyer, C., Roy, A.G., Best, J.L., 2006. Dynamics of a river channel confluence with discordant beds: Flow turbulence, bed load sediment transport and bed morphology. J. Geophys. Res. Earth Surface 111(F4). https://doi.org/10.1029/2005JF000458.

Bradbrook, K.F., Lane, S.N., Richards, K.S., Biron, P.M., Roy, A.G., 2001. Role of bed discordance at asymmetrical river confluences. J. Hydraul. Eng. 127(5), 351−368. https://doi.org/10.1061/(ASCE)0733-9429(2001)127:5(351).

Bradbrook, K.F., Lane, S.N., Richards, K.S., Biron, P.M., Roy, A.G., 2010. Large eddy simulation of periodic flow characteristics at river channel confluences. J. Hydraul. Res. 38(3), 207−215. https://doi.org/10.1080/00221680009498338.

Constantinescu, G., Miyawaki, S., Rhoads, B., Sukhodolov, A., 2012. Numerical analysis of the effect of momentum ratio on the dynamics and sediment-entrainment capacity of coherent flow structures at a stream confluence. J. Geophys. Res. Earth Surface 117(F4). https://doi.org/10.1029/2012JF002452.

Constantinescu, G., Miyawaki, S., Rhoads, B., Sukhodolov, A., 2014. Numerical evaluation of the effects of planform geometry and inflow conditions on flow, turbulence structure, and bed shear velocity at a stream confluence with a concordant bed. J. Geophys. Res. Earth Surface 119(10), 2079−2097. https://doi.org/10.1002/2014JF003244.

Creëlle, S., Schindfessel, L., De Mulder, T., 2017. Modelling of the tributary momentum contribution to predict confluence head losses. J. Hydraul. Res. 55(2), 175−189. https://doi.org/10.1080/00221686.2016.1212941.

De Serres, B., Roy, A.G., Biron, P.M., Best, J.L., 1999. Three-dimensional structure of flow at a confluence of river channels with discordant beds. Geomorphology 26(4), 313−335. https://doi.org/10.1016/S0169-555X(98)00064-6.

Đorđević, D., 2013. Numerical study of 3D flow at right-angled confluences with and without upstream planform curvature. J. Hydroinf. 15(4), 1073−1088. https://doi.org/10.2166/hydro.2012.150.

Dubief, Y., Delcayre, F., 2000. On coherent-vortex identification in turbulence. J. Turbul. 1. https://doi.org/10.1088/1468-5248/1/1/011.

Gualtieri, C., Filizola, N., Oliveira, M., Santos, A.M., Ianniruberto, M., 2018. A field study of the confluence between Negro and Solimões rivers, Part 1: Hydrodynamics and sediment transport. Compt. Rendus Geosci. 350(1−2), 31−42. https://doi.org/10.1016/j.crte.2017.09.015.

Hager, W.H., 1987. Discussion of "separation zone at open-channel junctions" by James L. Best and Ian Reid (November, 1984). J. Hydraul. Eng. 113(4), 539−543. https://doi.org/10.1061/(ASCE)0733-9429(1987)113:4(539).

Huang, J., Weber, L.J., Lai, Y.G., 2002. Three-dimensional numerical study of flows in open-channel junctions. J. Hydraul. Eng. 128(3), 268−280. https://doi.org/10.1061/(ASCE)0733-9429(2002)128:3(268).

Hunt, J.C.R., Wray, A., Moin, P., 1988. Eddies, stream, and convergence zones in turbulent flows. In: Proceedings of the Summer Program. Center for Turbulence Research, Stanford University, Stanford.

Kara, S., Kara, M.C., Stoesser, T., Sturm, T.W., 2015. Free-surface versus rigid-lid LES computations for bridge-abutment flow. J. Hydraul. Eng. 141(9), 04015019. https://doi.org/10.1061/(ASCE)HY.1943-7900.0001028.

Karami, H., Farzin, S., Sadrabadi, M.T., Moazeni, H., 2017. Simulation of flow pattern at rectangular lateral intake with different dike and submerged vane scenarios. Water Sci. Eng. 10(3), 246−255. https://doi.org/10.1016/j.wse.2017.10.001.

Kennedy, J.F., 1983. Reflections on rivers, research, and rouse. J. Hydraul. Eng. 109(10), 1253−1271. https://doi.org/10.1061/(ASCE)0733-9429(1983)109:10(1253).

Kennedy, B.A., 1984. On Playfair's law of accordant junctions. Earth Surf. Process. Landforms 9(2), 153−173. https://doi.org/10.1002/esp.3290090207.

Keylock, C.J., Constantinescu, G., Hardy, R.J., 2012. The application of computational fluid dynamics to natural river channels: Eddy resolving versus mean flow approaches. Geomorphology 179, 1−20. https://doi.org/10.1016/j.geomorph.2012.09.006.

Konsoer, K.M., Rhoads, B.L., 2014. Spatial-temporal structure of mixing interface turbulence at two large river confluences. Environ. Fluid Mech. 14(5), 1043−1070.

Lane, S.N., Hardy, R.J., Ferguson, R.I., Parsons, D.R., 2005. A framework for model verification and validation of CFD schemes in natural open channel flows. In: Bates, P.D., Lane, S.N., Ferguson, R.I., eds., Computational Fluid Dynamics: Applications in Environmental Hydraulics. John Wiley & Sons, Chichester.

Lewis, Q.W., Rhoads, B.L., 2018. LSPIV measurements of two-dimensional flow structure in streams using small unmanned aerial systems: 1. Accuracy assessment based on comparison with stationary camera platforms and in-stream velocity measurements. Water Resour. Res. 54(10), 7981−7999. https://doi.org/10.1029/2018WR022551.

Luo, H., 2017. Numerical Investigations of Flow Behavior and Energy Losses in Open Channel Junctions. Ph. D. Dissertation. University of Illinois at Urbana-Champaign, Champaign.

McSherry, R.J., Chua, K.V., Stoesser, T., 2017. Large eddy simulation of free-surface flows. J. Hydrodyn. 29(1), 1−12. https://doi.org/10.1016/S1001-6058(16)60712-6.

Pope, S.B., 2004. Ten questions concerning the large-eddy simulation of turbulent flow. New J. Phys. 6(35). https://doi.org/10.1088/1367-2630/6/1/035.

Pouchoulin, S., Ramos, P.X., Mignot, E., Schindfessel, L., De Mulder, T., Riviere, N., 2018. Discussion of "Tang, H., Zhang, H., and Yuan, S. (2018). Hydrodynamics and contaminant transport on a degraded bed at a 90-degree channel confluence. Environmental Fluid Mechanics, 18(2), 443−463". Environ. Fluid Mech. 18(5), 1293−1295. https://doi.org/10.1007/s10652-018-9612-x.

Ramos, P.X., Schindfessel, L., Pêgo, J.P., De Mulder, T., 2018. Influence of bed discordance on head losses in an open channel confluence. In: Proceedings of the 5th IAHR Europe Congress New Challenges in Hydraulic Research and Engineering. IAHR, Trento, pp. 107−108. https://doi.org/10.3850/978-981-11-2731-1_060-cd.

Ramos, P.X., Schindfessel, L., Pêgo, J.P., De Mulder, T., 2019. Flat vs. curved rigid-lid LES computations of an open-channel confluence. J. Hydroinf. 21(2), 318−334. https://doi.org/10.2166/hydro.2019.109.

Rice, S.P., Roy, A.G., Rhoads, B.L., 2008. River Confluences, Tributaries and the Fluvial Network. John Wiley & Sons, Chichester.

Rodi, W., Constantinescu, G., Stoesser, T., 2013. Large-eddy Simulation in Hydraulics. CRC Press, Balkema.

Rodi, W., 2017. Turbulence modeling and simulation in hydraulics: A historical review. J. Hydraul. Eng. 143(5), 03117001. https://doi.org/10.1061/(ASCE)HY.1943-7900.0001288.

Schindfessel, L., Creëlle, S., De Mulder, T., 2015. Flow patterns in an open channel confluence with increasingly dominant tributary inflow. Water 7(9), 4724−4751. https://doi.org/10.3390/w7094724.

Schindfessel, L., 2017. Numerical and Experimental Modeling of the Hydrodynamics of Open Channel Confluences with Dominant Tributary Inflow. Ph. D. Dissertation. Ghent University, Ghent.

Umar, M., Rhoads, B.L., Greenberg, J.A., 2018. Use of multispectral satellite remote sensing to assess mixing of suspended sediment downstream of large river confluences. J. Hydrol. 556, 325−338. https://doi.org/10.1016/j.jhydrol.2017.11.026.

Weber, L.J., Schumate, E.D., Mawer, N., 2001. Experiments on flow at a 90° open-channel junction. J. Hydraul. Eng. 127(5), 340−350. https://doi.org/10.1061/(ASCE)0733-9429(2001)127:5(340).

Yuan, S.Y., Tang, H.W., Xiao, Y., Qiu, X.H., Xia, Y., 2017. Water flow and sediment transport at open-channel confluences: An experimental study. J. Hydraul. Res. 1−18. https://doi.org/10.1080/00221686.2017.1354932.

Yuan, S.Y., Tang, H.W., Xiao, Y., Chen, X., Xia, Y., Jiang, Z.Y., 2018. Spatial variability of phosphorus adsorption in surface sediment at channel confluences: Field and laboratory experimental evidence. J. Hydro Environ. Res. 18, 25−36. https://doi.org/10.1016/j.jher.2017.10.001.